Département Sciences de la Matière
École Normale Supérieure de Lyon
Université Claude Bernard Lyon 1

Internship Report
Théo Reymermier
Master 1 Physique

Timing coincidence trigger setup

ANUBIS project (AN Underground Belayed In-Shaft search experiment)

Abstract : *Construction of a trigger setup to measure the efficienty, and other performance parameters of* ***Resistive Plate Chambers*** *(RPC) detectors. The RPC detector is used (outside the context of the internship) for the ANUBIS detector, in search of long-lived particles. The sensitivity to long-lived particles can be significantly improved by an additional detector at the large hadron collider. The setup consists of two scintillators placed on top of each other and connected by a temporal coincidence device in order to detect the passage of particles (muons). The RPC whose efficiency we wish to measure is then placed between the two scintillators, and, using a new temporal coincidence device, we find the number of particles that the detector and the scintillators are measuring, which we then compare to the total number of particles measured by the scintillators.*

August 29, 2022

internship supervised by:
Oleg Brandt
obrandt@hep.phy.cam.ac.uk
Cavendish Laboratory U. of Cambridge
JJ Thomson Avenue Room: 950 (Rutherford)

Acknowledgements

I would like to thanks members of the Cambridge HEP group for their welcome and their help throughout my internship.

I wish especially to thank Steve Wotton, who helped me with the whole creation of the device. As well as my tutor, Oleg Brandt, for his invaluable help, and his many advice.

I also wish to thank my friend Evrard Emonot, for his precious help with the code and the simulation.

Finally, I also thank Alain Gabet, for his numerous and precious lessons.

Table of contents

1 Introduction

One of the biggest questions in physics, and especially in particle physics, concerns the nature of certain particles that are not part of the **Standard Model** (SM), and which would require a redefinition of the current model, and possibly explain, for example, the origin of dark matter. Some of the theories, called **supersymmetric theories** (SUSY), implies the existence of superpartner for each particle of the standard model, which differs from the original particle by a spin 1/2 (bosons-fermion transformation).
The ANUBIS project concerns the search for particles (possibly supersymmetric) with macroscopic lifetime (Long-lived particles or LLP). The current **Large Hadron Collider** (LHC) detectors are not built for this kind of study, their size limiting the study of **long-lived (neutral) particles**. ANUBIS objective would be to use the PX14 (Fig.1) service shaft of ATLAS[1] (which is not instrumented yet), to place an additional tracking detector and increase the sensitivity.

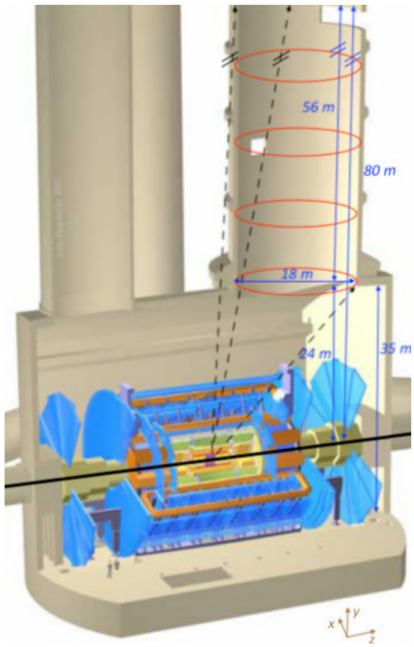

Figure 1: Schematic view of the UX15 cavern with the ATLAS detector and the access shafts PX16, PM15, and PX14 (from left to right). The position of ANUBIS would be in the PX14 shaft, with the dimension shown by the blue arrow and red ellipses. Figure from Ref.[1]

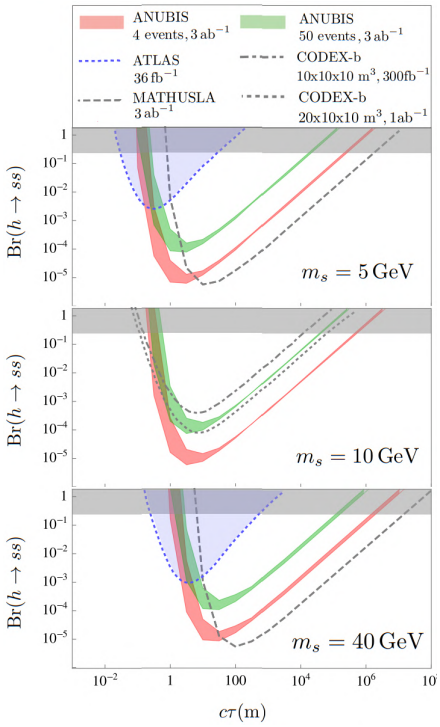

Figure 2: Projected sensitivity of ANUBIS, CODEX-b Ref.[2], and MATHUSLA Ref.[3] for LLPs for Higgs decays $h \to ss$ with different LLP masses $m_s = 5, 10$ and 40 GeV at the HLLHC with a center-of-mass energy of 14 TeV. The filled area (except the blue one that show ATLAS current possibility) show the effect of adding the ANUBIS detector beyond the muon spectrometer .Figure from Ref.[1].

Fig.2 shows, for Higgs decays with differents masses of long-lived scalar, s (Fig.3), that the accessible branching ratio become lower and could make it possible to search outside the sectors currently studied by ATLAS (the blue part of the figure).
LLP are not necessarily particles of BSM theories, there are already several within the SM (Fig.4) .

[1] **ATLAS** is a detector, at the LHC, used for research around the higgs boson, dark matter, and new dimensions.

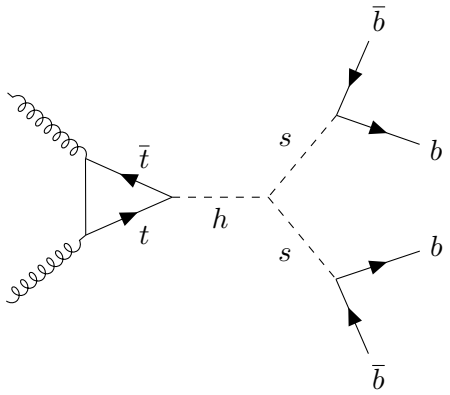

Figure 3: Feynman diagram for $h \to ss$. h is the higg boson, t the top quark, b the bottom quark and s the long-lived scalar.

To search for LLP **Beyond the Standard Model** (BSM), ANUBIS will use an indirect detection method (see section 2.1.3). For example, to detect a neutral supersymmetric particle, like those shown in Fig.5 and Fig.6, it will try to detect charged particles, using the RPC detector, and reconstruct the trajectories to go back to the vertex at the origin of these particles.
Then, using the information collected by ATLAS, we will know if the particle at the origin of this vertex has been detected by ATLAS (and is therefore a known particle, such as a neutral pion for example), or not, and is therefore possibly a new LLP particle that ATLAS is unable to spot.
To detect the tracks of charged particles, ANUBIS would be equipped with an RPC detector, whose efficiency remains to be determined. Our objective here is to measure this efficiency using a tracking setup, made up of scintillators. Our main goal was to determine the best location for the **Silicon Photomultiplier** (SiPM) on the scintillator, to measure the efficiency, as well as to assemble the setup, optimizing the location of the electronics as much as possible.
Building a device to measure the efficiency of a detector will in particular help to choose a gas with the best performance. Moerever, the objective in the choice of gas is also important for the environment. Indeed, the gases normally used in RPC detectors have a very high carbon footprint, 1400 times higher than CO_2. The goal here will be to find a gas with similar efficienc, measured using our setup, but with a lower carbon footprint.
In the first place, the report will give a short introduction to LLP, and the detector (With more details on the scintillator part, as this is what we will be using for my project). Then we will introduce the material used for the construction of the tracking setup and coincidence setup that we used to track the particles and determine the efficiency. Finally, we will discuss the results obtained, measures and simulations, and the overall assembly finalized.

2 Long lived particles and detector

2.1 Long lived particles

The Standard Model of particle physics explains a large part of the microscopic phenomena that can be observed and also part of the macroscopic phenomena, like weak decays, quark states, fusion in stars, etc., by considering interactions between elementary particles, exchanging energy and momentum via other particles, called gauge bosons. Problems such as the existence of dark matter, or the mass hierarchy problem, the mass gap between particle generations, still remains, and many BSM theories try to explain these questions. To understand new phenomena, two ways are under investigation, either to seek for a new way of interacting between the particles of the standard model, or then, as we will see, to search for new particles, interacting differently. We will explore in this report the hypothesis of the existence of new particles.

2.1.1 Lifetime of a particle

The average life time of a particle is a very important piece of information, because it influences in a very important way the behavior of the particles, as well as their detection. It is very strongly related to the mass of the particle. It is defined as the average time before the particle decays into other particles.

Proper lifetime of a particle

The proper lifetime of a particle X (with a mass m_X), called τ is given (in natural units) by (Ref.[4]) :

$$\tau^{-1} = \frac{1}{2m_X} \int |\mathcal{M}(m_X \longrightarrow \{p_X\})|^2 d\Pi_f \tag{1}$$

$\mathcal{M}(m_X \to \{p_X\})$ correspond to the matrix element of every possible decays of the particle X into $\{p_X\}$, the decay products. $d\Pi_f$ is the Lorentz-invariant phase space which is different for each decay.

2.1.2 Assumptions about particle lifetime

In general, these theories consider that the new particles appearing in the theory have a very short lifetime to explain the fact that they have not been observed yet. Such considerations impose certain conditions on the equation giving τ (Equation 1). Indeed, to have particles with a short lifetime, it is therefore necessary either to have a large phase space, or to have a large matrix element $\mathcal{M}$.

However, these particles can also be metastable, or even stable, like many particles of the Standard Model (Fig.4). Some encouraging results from theories begin to solve quite efficently the problems of the standard model. They encourage us to look in areas not yet studied. The challenge of these areas being the significant presence of SM backgrounds as shown in Fig4, as the detectors were not created for this purpose.
Fig.4 shows that some particles of the standard model are stable or metastable, the same goes for many particles from models beyond the standard model (such as supersymmetry). To obtain long-lived particles, it is necessary this time, according to equation 1, to consider a small matrix element M, or a small Lorentz-invariant phase space.
The predicting models for the existence of these particles will not be studied here, since we use muons[2] for measuring the detector efficiency, which are SM LLP (Fig.4), given their presence through cosmic rays. A brief overview of these models is available in appendix A.

[2]explanations of this choice are given in Appendix D

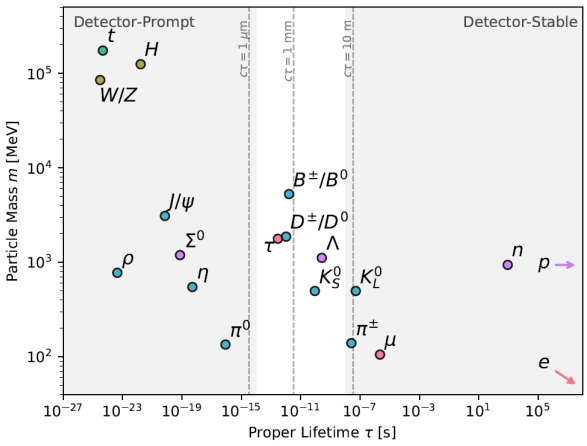

Figure 4: Standard model particle spectrum as function of mass and proper lifetime. If decay occurs at larger distances, $10^{-10}\,m$ the particle is called **detector-Stable**, if the distance between production points and decay points is smaller than the spatial resolution of the detector, the particle is called **Detector-Prompt**. Figure from Ref.[4]

To summarize briefly, the objective is to understand when the conditions we proposed on equation 1 are satisfied. To obtain a small matrix element, it is possible, for example, to consider a small symmetry breaking.

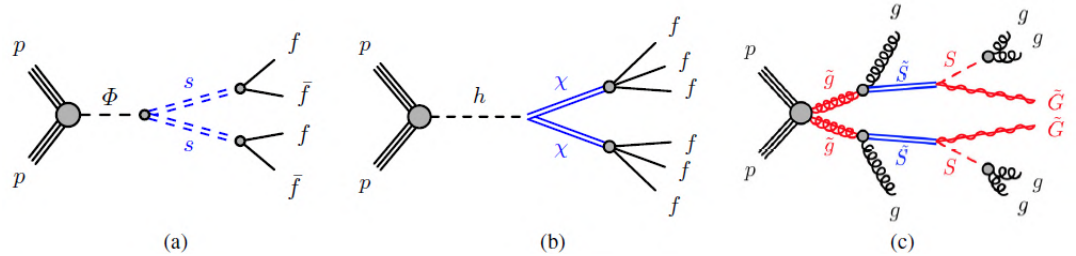

Figure 5: Examples of Feynman diagrams proposed for the creation of LLP in BSM models. (a) scalar portal model (b) Higgs portal baryogenesis model (c) stealth SUSY model. f are fermions of the Standard-model, g the gluons, χ the neutralino, S the singlet, $\tilde{S}$ the singlino, h the Higgs boson, $\tilde{g}$ the gluino, $\tilde{G}$ the gravitino. LLPs are shown in double blue lines. Figure from Ref.[5].

Fig.5 represents different possible Feynman diagrams for LLP production in a proton-proton collider, which differ according to the theories used. As explained in the introduction, we see that these particles disintegrate into particles of the standard model with the exception of the gravitino, it is therefore possible, by indirect detection, to go back to the vertex of the creation of these particles, and to deduce the properties of these supersymmetric particles.
This is the goal of ANUBIS. The models used for the Feynman diagrams in Fig.5 and Fig.6 will not be introduced here, as they are difficult to describe synthetically and far beyond the project. However, they are very well explained in Ref.[2]. Another example, in Fig.6, at an hadron collider, involves a long-lived neutralino.

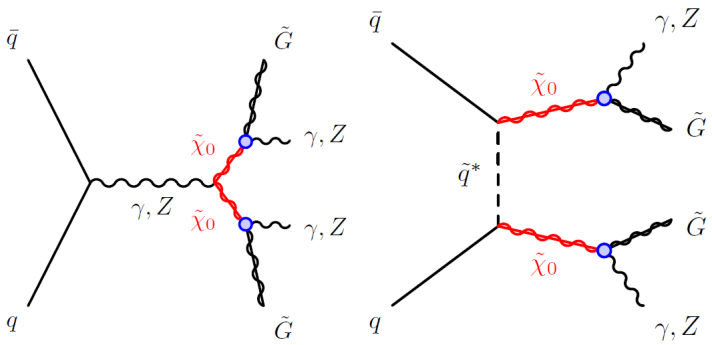

Figure 6: Feynman diagram producing long-lived neutralino $\tilde{\chi}_0$ (s-channel in the left, and t-channel in the right with a squark). The blue circle denotes the vertex that makes the neutralino long-lived. γ is the photon, Z the Z^0 boson, q a quark, and $\tilde{G}$ the gravitino. Figure from Ref.[4].

2.1.3 Detection

LLP detection methods are categorized in two classes : **direct detection** and **indirect detection**. The first one seek for direct interaction of the particle with the detector, for example with Anomalous ionization, or delayed detector signals. Whereas in the indirect detection, the objectif is to reconstruct the decay of the particle (into particles of the standard model).

In the search for LLP, when the detection is indirect, the particle passes through the different parts of the detector without interacting. The only means of detection here is to wait for the particle to decay.

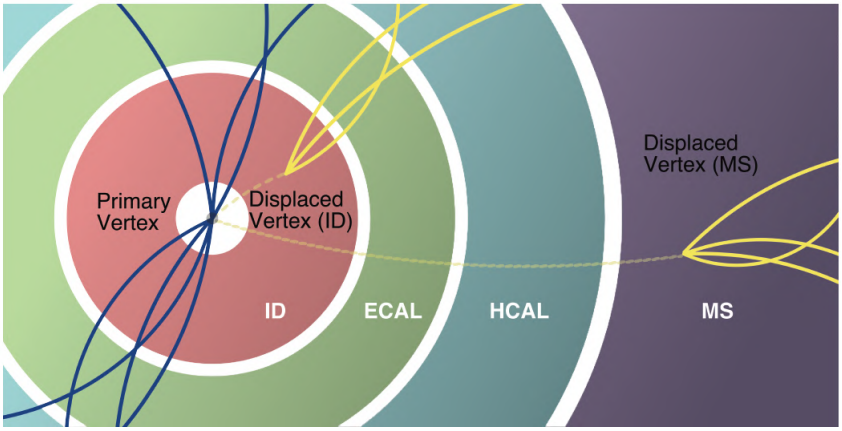

Figure 7: Primary and Displaced vertices (in the **inner detector**, ID, and the **muon system**, MS). Figure from Ref.[4].

Fig.7 shows us that the displayed vertex can appear in different parts of the detector, up to the muon system and before this new vertex, the particle does not seem to have interacted, therefore remains impossible to detect.
If we rely on the supersymmetric theories[3] the displayed vertex can appear beyond the muon system, hence the interest in placing the ANUBIS detector, which will capture these interactions, which crosses ATLAS without interaction.

[3]Other theoretical framework also generate LLPs, but they will not be studied here

2.2 Detectors

2.2.1 RPC detector

RPC are widely used in particle physics expermiments (to track particles). They consist of two parallel plates (anode and cathode, Fig.8a) separated by some gas. When a *charged* particle passes through the gas, it creates an avalanche of electrons (Fig.8b), which are sent on an external metallic plate, which allows us to know, roughly, the *charged* particle's momentum and the place where it passed.

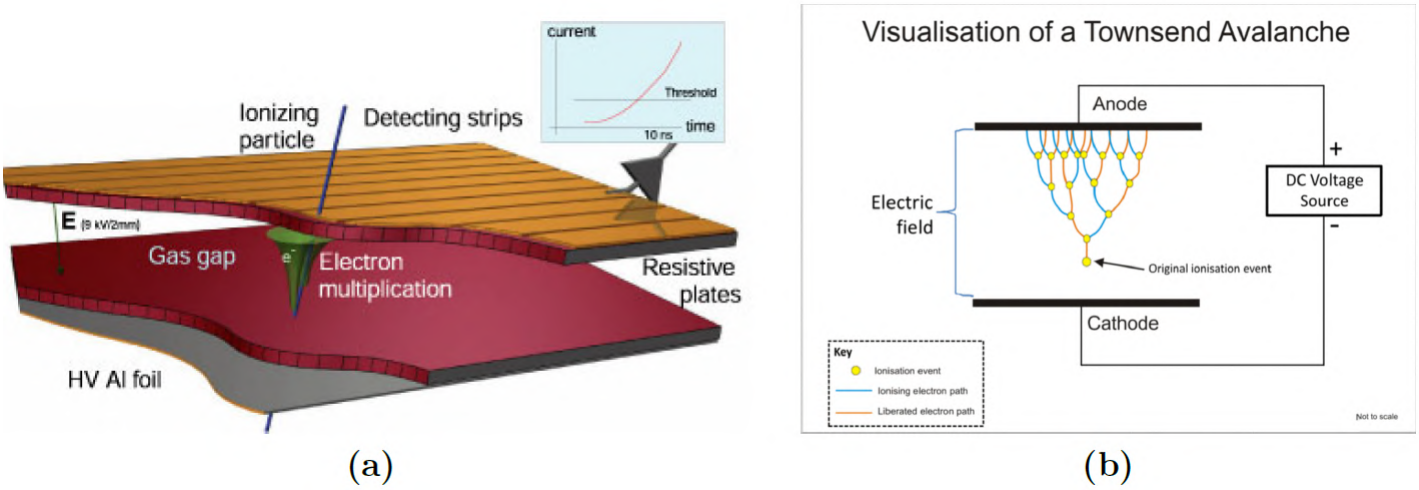

Figure 8: (a) Explanatory diagram of an RPC (b) Evolutionary diagram of a Townsend avalanche, detection is done at the anode. Figure from Ref.[6].

These detectors will not be studied in detail here (outside the scope of this internship), but it is the type of detectors (in ANUBIS) whose efficiency will be measured using our tracking setup (made with scintillators). One of the most important elements (and the starting point) in the study of RPCs is the initial ionization. It is due to the passage of a charged particle in the gas, which interacts and loses energy, in particular by ionization (Equation 2).

Bethe formula

For a charge particle, with a mass $M >> m_e$ (m_e the mass of the electron), we have the mean energy loss of the particle throught excitation and ionisation :

$$\left\langle -\frac{dE}{dx} \right\rangle = Kz^2 \frac{Z}{A}\frac{1}{\beta^2}\left(\frac{1}{2}\ln\left(\frac{2m_e c^2\beta^2\gamma^2 T_{max}}{I^2}\right) - \beta^2 - \delta(\beta\gamma)\right) \tag{2}$$

With $K = 4\pi N_A r_e^2 m_e c^2$ and $r_e = \frac{e^2}{4\pi\epsilon_0 m_e c^2}$ the electron radius.

- e and z the charge of the electron and the incident particle.
- Z, A the atomic number and mass.
- β, c, γ the velocity of the particle, the speed of light and the Lorentz factor.
- $T_{max} = \frac{2m_e p^2}{M^2+2\gamma m_e M+m_e^2}$ the maximum energy transfer in a single collision (p is the momentum of the particle), I the mean excitation energy of the absorbing medium.
- δ the density effect correction.
- N_A the Avogadro's number, and ϵ_0 the dielectric constant (in vacuum).

Equation from Ref.[6].

2.2.2 Scintillator and Silicon Photomultipliers

A scintillator is a material that emits light when a charged particle (such as an electron, or muon) passes through it (or more generally when it absorbs an ionizing ray). It is important to know the wavelength of the photon emitted by the scintillator, because the choice of the SiPM will depend on this value, in order to optimize the detection of the photon.

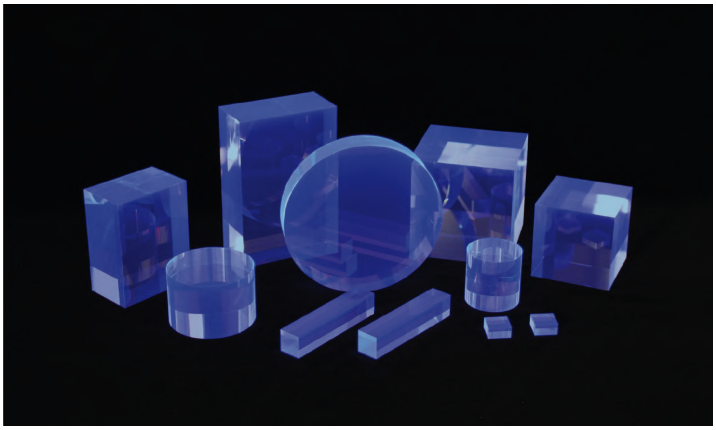

Figure 9: Photography of several scintillators, of several different shapes. Figure from Ref.[7].

An example of (inorganic) scintillators is shown in Fig.9, however, in view of their usefulness, they are always surrounded by a wrapping, in order to preserve them from external light.
The photon emitted by the Scintillator will then be absorbed in the silicon part of the SiPM, in order to create an electron-hole pair, which will then be amplified to create an output signal.
The silicon works in Geiger mode, meaning that a single photon can emit an avalanche, and turn into a macroscopic current. To place itself in Geiger mode (Fig.10), the SiPM needs a high electric field, so that when a photon passes, the pair of particle-antiparticle (electron-hole) produced gains enough kinetic energy for a second pair. (by impact ionization). And so on, until an avalanche is generated.

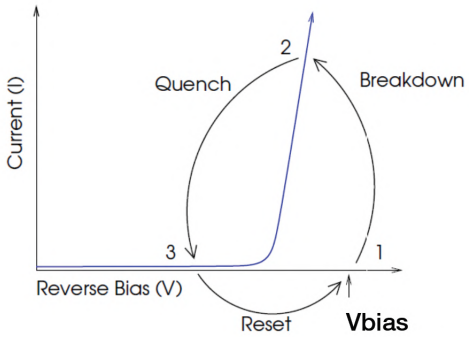

Figure 10: Silicon photomultiplier working in Geiger mode. The breakdown appear when a photon triggers a self-perpetuating ionization cascade in the depletion area. The current is then stopped (quenched), and reset, as if it had an on/off mode. Figure from Ref.[8].

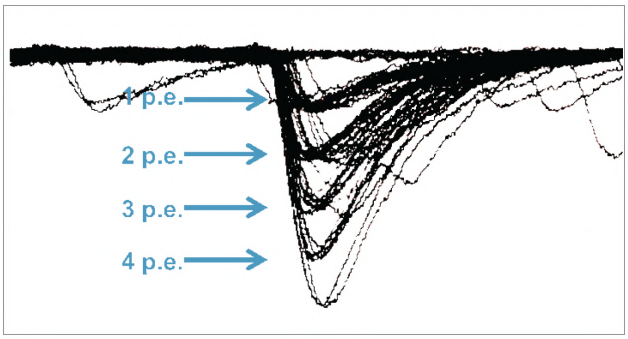

Figure 11: Image of an oscilloscope showing the signal emitted by a pulse of low intensity light. Figure from Ref.[8].

When several photons hit the silicon, the amplitudes are added, hence the amplitude differences for the signals in Fig.11. Many factors determine the performance of a SiPM.

Performances parameters

A silicon Photomultiplier has many parameters, as Breakdown voltage, gain, **Photon Detection Efficiency** (PDE), **Dark Count Rate** (DCR), optical crosstalk, after pulsing, etc. These parameters are well describe in Ref.[8].

We will only deal here with DCR, which are the main source of noise in a SiPM. This noise corresponds to thermally generated electrons, which create avalanches (as if a photon was detected) and are independent of the passage of light. Several methods are possible to remove this noise :

• Choosing a threshold beyond the amplitude of the signals due to the DCR, which completely eliminates this noise, but can also reduce the possibility of detecting the signal we are trying to measure.

• Measuring this noise (which is comprised of a series of pulses) in the absence of light, in order to adjust our device so it doesn't take this signal into account.

As the notion of PDE will intervene later in our study, to compare two SiPMs, it is necessary to define it here.

Photon Detection Efficiency

The PDE is a measure of the sensitivity of the SiPM (function of the wavelength). It is defined by :

$$PDE(\lambda, V) = \eta(\lambda).\epsilon(V)F \tag{3}$$

Equation from Ref.[8]. $\eta(\lambda)$ is the quantum efficiency of the silicon (possibiliy of a photon to create a electron-positron pair), and $\epsilon(V)$ the avalanche initiation probability. F is the fill factor of the device, which tells us the percentage of the sensor sensitive to light. Indeed, all the SiPM sensor surface area is not sensitive to the passage of a photon, since it is necessary to separate each cell from its neighbors to prevent a photon from creating two avalanches in two different cells.

3 Study of the components

The device we have assembled has several components, scintillators to detect (the • in Fig.12 represente the detection) the passage of muons (blue line in Fig.12), by photon emission. The photons are then detected by the SiPMs, and transformed into an electrical signal, which is then sent to a coincidence setup, to defenciate the muon detection from the noise signal. The coincidence 1 in Fig.12 works as a OR logical gate for SiPM on the same scintillator, and AND logical gate between the two scintillators.

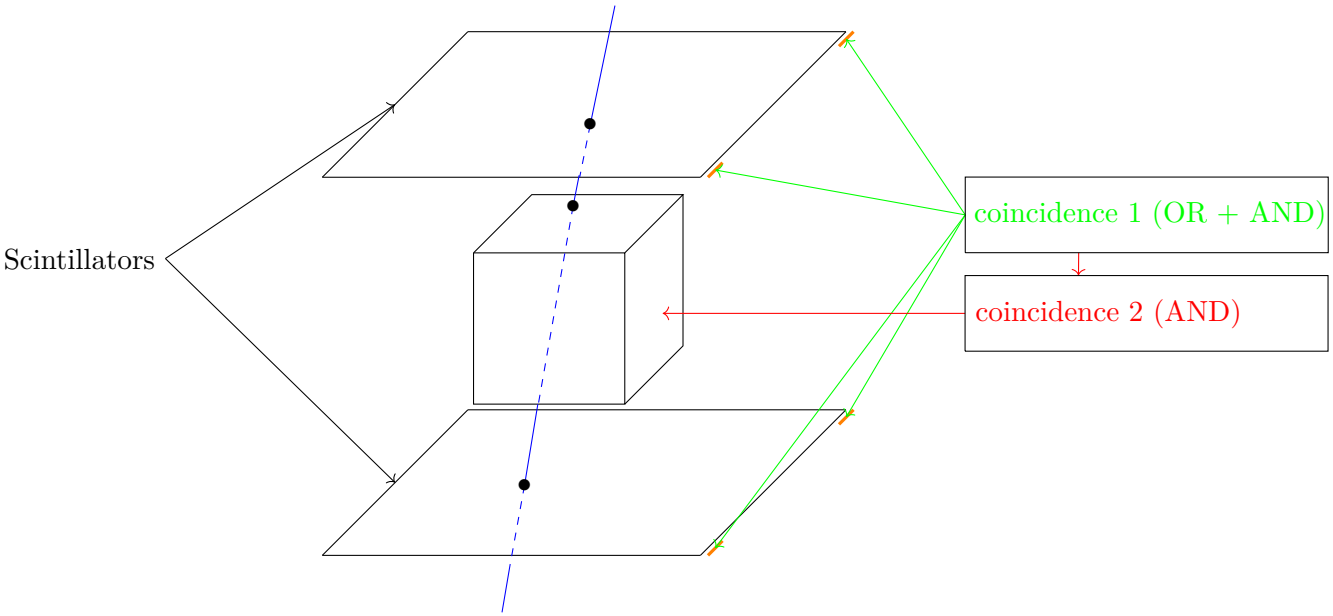

Figure 12: Simplified diagram of the device, with the SiPMs in orange, coordinating using a first coincidence setup (coincidence 1, in green), itself linked to a second (coincidence 2, in red) allowing coincidence with the device (the cube) of which we want to know the efficiency.

While we have assembled the electronic part of the setup, the mechinal part of the device is built by the mechanical workshop of the university of Cambridge.

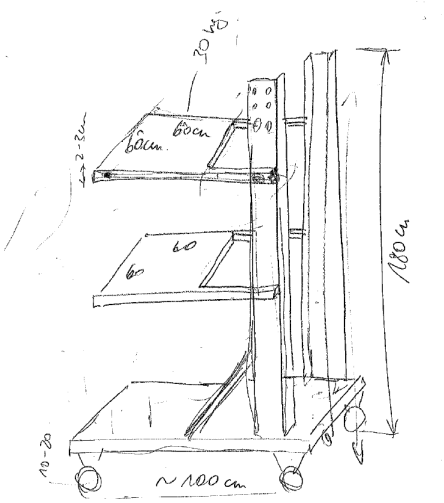

Figure 13: Drawing of the final device showing the mechanical part. Drawn by my tutor.

As presented by the explanatory diagram (Fig.12), the scintillators will be located at the top and at the bottom. The RPC will be at the center. The questions concerning the mechanical part mainly lie in the choice of placement of the electronics. We want a high efficiency and low noise for the coincidence setup. We also need to be careful as the electronics can interfere with the measurement, which should be avoided as much as possible.

3.1 Silicon Photomultiplier

Before any measurement with the SiPMs, and each time a board is mounted with the SiPM on it, we first check the emitted signal using an oscilloscope. Coherent signal should behave as in Fig.11.
Fig.14 shows that the SiPMs seem to work well. Of course, this analysis is not quantitative, but allows to identify abnormal functioning.
The SiPM is an important part of our setup, since efficiency largely depends on it. In particular, the simulation that we created (see more detail in section 4) allowed us to optimally choose the SiPMs placements on the scintillator where the number of photons detected by the silicon is the most important.

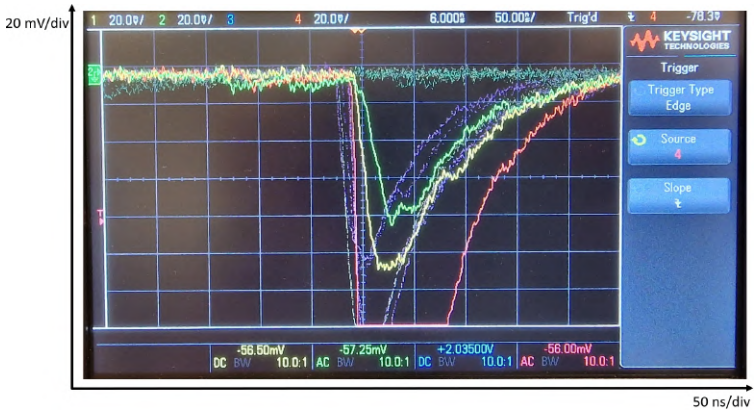

Figure 14: Illustrative image of an oscilloscope, showing different SiPMs in operation (each color corresponds to a different SiPM), receiving weak pulses of light.

Our simulation (Fig.15) reproduces the emission of photons during the passage of muons (Fig.12) by considering the muons in normal incidence. The choice of this incidence is natural, given that it corresponds to a minimum path of the muon within the silicon, and therefore a minimum of photon emission, which is a reasonable choice when seeking for the efficiency of the device.

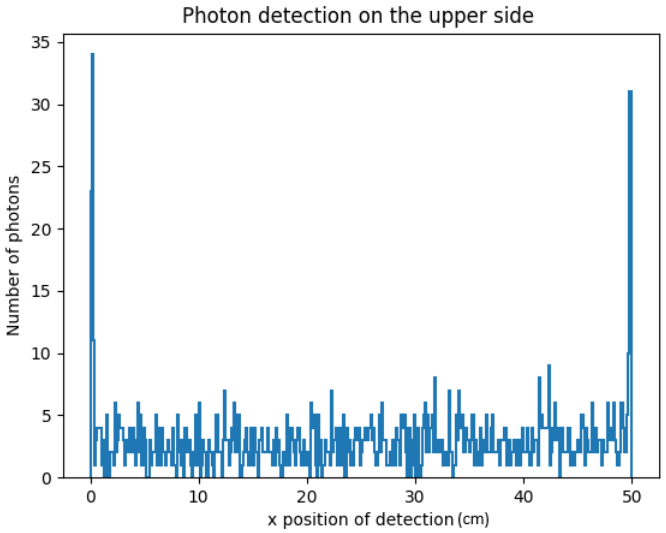

Figure 15: Numbers of photons that can be detected by a 3mm SiPM as a function of position along the top of the scintillator (simulation with 500 muons).

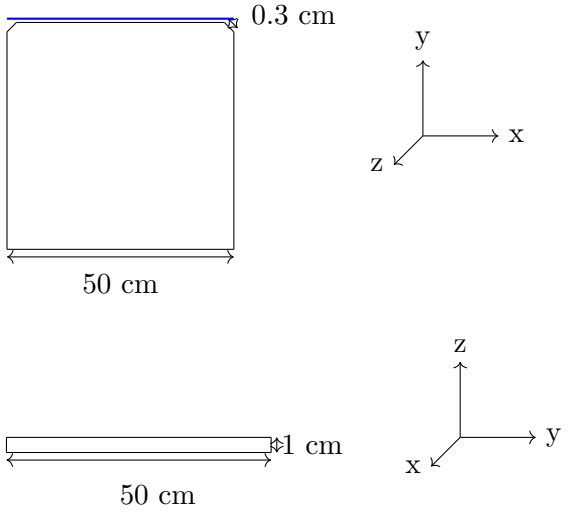

Figure 16: Diagram of the scintillator, the part corresponding to the results of Fig.15 is the upper side (blue line).

According to this simulation, which of course makes many approximations, the best locations for the SiPMs are therefore the two corners (shown in Fig.16) of the scintillators. This can be explained by the 45° cut made on these corners, which gives them a greater solid angle than the other locations, and therefore they can collect a greater number of photons, regardless of their origin.

We first thought of using only one SiPM, in order to limit the presence of electronics, and especially of wires. However, the average efficiency with a single SiPM did not exceed 60 %. So we decided to add another SiPM to the setup. Given the symmetries of the device, it seemed natural, having placed the first SiPM on a corner, to place the second on the second cut, in order to cover as much surface as possible, as it is the solid angle which matters the most for the efficiency. Of course, this result was expected, that's why we had planned two basic cuts, and the necessary electronic equipment.

3.1.1 Ketek PM3315-WB-B0

The first SiPMs tested are called Ketek. They were chosen for their high efficiency and their very low noise. All efficiency measurements, using the 10 x 10 cm tracking setup presented in section 4.2.1, were performed with these SiPMs.
The sensor is then mounted on a board (Fig.17, assembled on site) to generates a signal of about 0.8 V, classical limit for digitalisation, which is then sent to the coincidence setup, and digitally transformed (1 if detected, 0 otherwise).

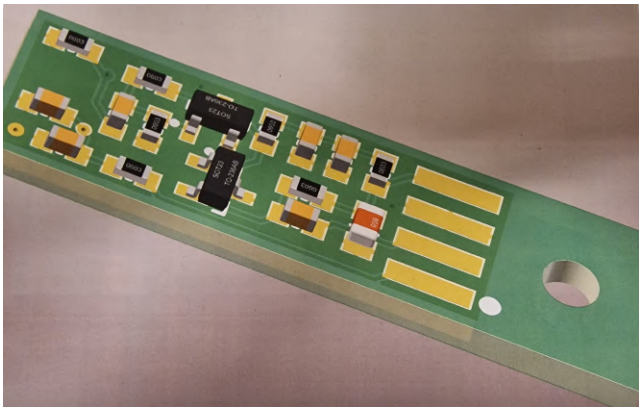

Figure 17: Photography of the board on which the SiPM is installed.

This board requires a 5 V power supply (for its operation), as well as another power supply of 30 V to create the high electric field on the SiPM. After the measurement of the efficiency for the first time, we decided to increase this 30 V to 32 V. Indeed, by changing this voltage, we increase the probability that a photon triggers an avalanche. However, we did not go beyond that, as it may increase certain noises, which was not discussed in detail (Optical Crosstalk, Afterpulsing...). The PDE is given in Fig.18.
The measurement presented in Fig.19 allows us to choose the right detection threshold, in order to obtain the best possible efficiency, without noise interference.
The way in which the noise indicated in Fig.19 are measured is quite simple, we take the device presented in section 4.2.1, and we place the tracking setup (composed of small scintillators) away from the scintillator on which the SiPMs are mounted, so that normally no muons can be detected by both scintillators at the same time. If "muons" are detected, then these are random coincidences due to noises, which are taken into account by the coincidence setup.

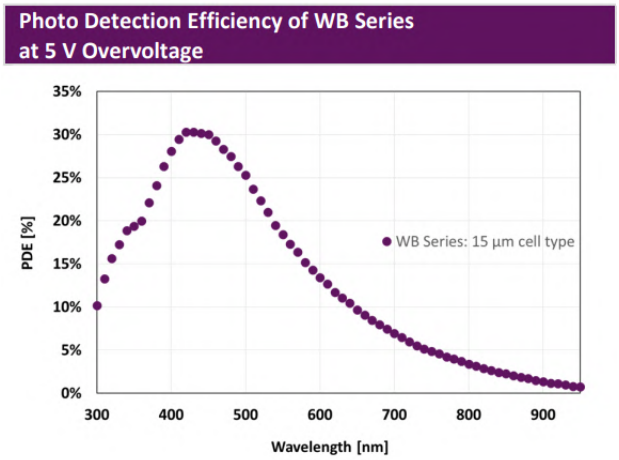

Figure 18: PDE of the Ketek SiPM as a function of wavelength (with 5V Overvoltage). The maximum is reached in 420 nm. Figure from Ref.[9].

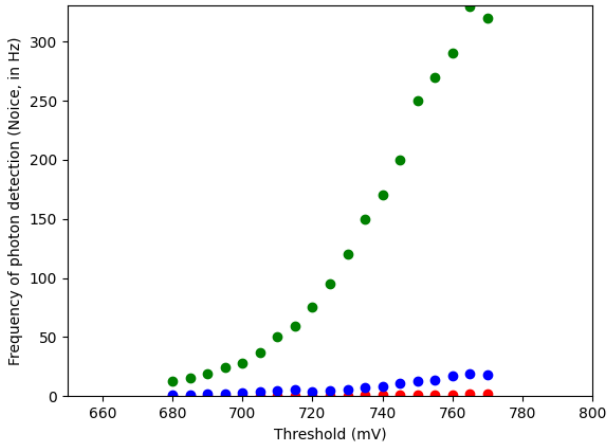

Figure 19: Noise (measured) of the Ketek SiPM as a function of the threshold voltage for this SiPM (presented in section 3). The red points were measured with a threshold of 680 mV for the tracking setup, 700 mV for the blue one and 720 mV for the green one.

3.1.2 Broadcom AFBR-S4N33C013

Broadcom SiPMs will be used for the final tracking setup, given their higher PDEs in the wavelength ranges we use (see Fig.18 and Fig.20). Another advantage is the noise which is much lower than the KETEK.
We observe in Fig.21 that placing the threshold at 700 V for the tracking setup, we can easily increase the acceptance threshold of the tested scintillator, without increasing the noise. The noises presented in Fig.21 allow us to know how to find the best efficiency, paying attention to the noises that can influence the measurements. To reduce these noises we do not count only on the threshold, but also on the wrapping on the scintillator, which allows the SiPM to receive (in theory) only the photons coming from the muons.

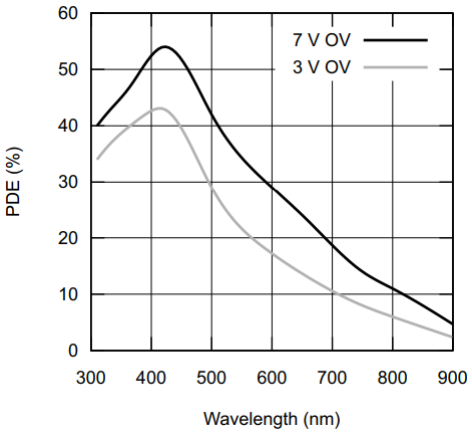

Figure 20: PDE of the Broadcoms SiPM as a function of wavelength (with differents overvoltage, 3 V and 7 V). Maximum reached in 420 nm. Figure from Ref.[10].

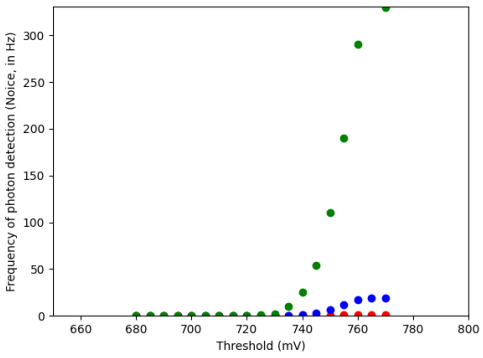

Figure 21: Noise (measured) of the Broadcom SiPM as a function of the threshold voltage for this SiPM (presented in section 3). The red points were measured with a threshold of 680 mV for the tracking setup, 700 mV for the blue one and 720 mV for the green one.

3.2 Scintillator

The Scintillator we used for our tracking setup is an EJ-200 (Ref.[7]), which has a long optical attenuation length and was therefore a good choice for our project, and the dimensions of our device (50×50 cm^2 for the scintillators).

PROPERTIES	EJ-200	EJ-204	EJ-208	EJ-212
Light Output (% Anthracene)	64	68	60	65
Scintillation Efficiency (photons/1 MeV e$^-$)	10,000	10,400	9,200	10,000
Wavelength of Maximum Emission (nm)	425	408	435	423
Light Attenuation Length (cm)	380	160	400	250
Rise Time (ns)	0.9	0.7	1.0	0.9
Decay Time (ns)	2.1	1.8	3.3	2.4
Pulse Width, FWHM (ns)	2.5	2.2	4.2	2.7
H Atoms per cm^3 ($\times 10^{22}$)	5.17	5.15	5.17	5.17
C Atoms per cm^3 ($\times 10^{22}$)	4.69	4.68	4.69	4.69
Electrons per cm^3 ($\times 10^{23}$)	3.33	3.33	3.33	3.33
Density (g/cm^3)	1.023	1.023	1.023	1.023
Polymer Base	Polyvinyltoluene			
Refractive Index	1.58			
Softening Point	75°C			
Vapor Pressure	Vacuum-compatible			
Coefficient of Linear Expansion	7.8×10^{-5} below 67°C			
Temperature Range	-20°C to 60°C			
Light Output (L.O.) vs. Temperature	At 60°C, L.O. = 95% of that at 20°C No change from -60°C to 20°C			

Figure 22: Properties of differents scintillators. Figure from Ref.[7].

We used the data from Fig.22 for our simulation, especially for the refractive index of the medium, which we used to determine the critical angle of the Scintillator-air interface. We will later see that for coincidence, the light attenuation length is also important
One important parameter is also the emission spectrum of the scintillator, which, due to the choice we made, reaches its maximum at 425 nm, as shown in Fig.23. This corresponds to the maximum sensitivity for the SiPM. This important data ensure a match between the spectra of the scintillator and the SiPM, allowing to obtain the greatest possible efficiency.

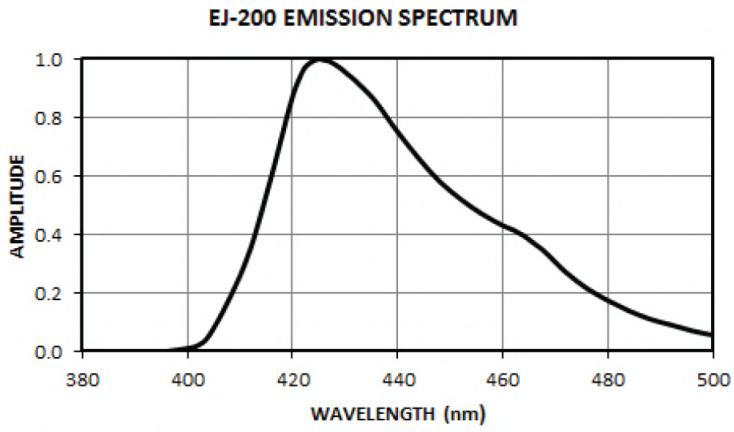

Figure 23: Photon emission spectrum within the scintillator, as a function of wavelength. Figure from Ref.[7].

3.3 Coincidence Setup

The signal obtained by the SiPM presented previously is then transformed into a digital signal using our coicidence setup (Fig.24).

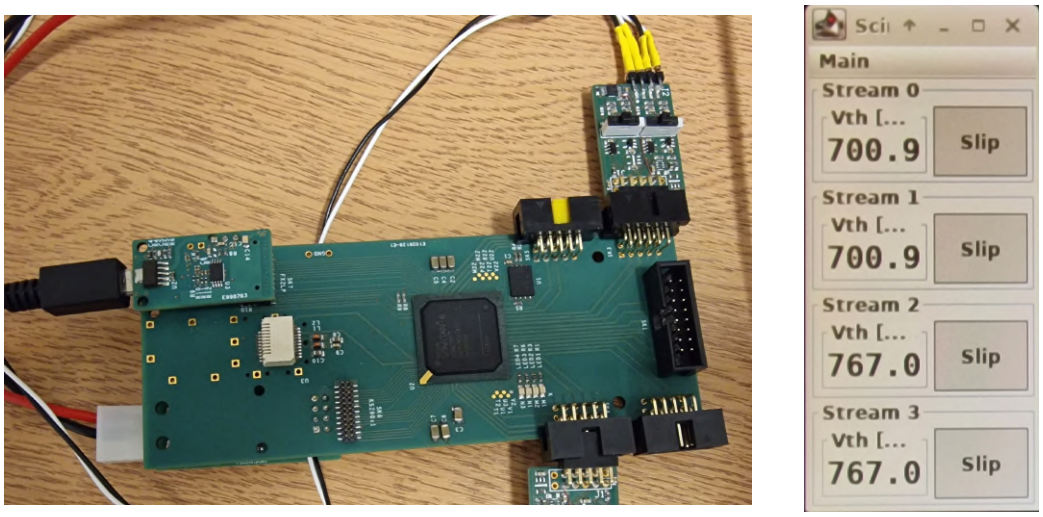

(a) (b)

Figure 24: (a) Picture of the Coincidence setup, where the white cables are connected to the SiPMs. The board on which they are connected allows digitization. The coincidence is done on the main board. (b) Picture of the software window allowing to choose the threshold, i.e. to discriminate the signals, in order to eliminate the noise.

The choice of the threshold is made after analysis of the SiPM noises (see section 3.1). Then comes the coincidence, which is done first between the two scintillators forming the tracking setup, and then with the third scintillator with unknown efficiency that is to be measured.

In the example presented in Fig.25, we see that 120 muons are detected by the tracking setup, among which 106 are also detected by the 3rd Scintillator. The efficiency is therefore evaluated at 88%. However, the time window during which the detection is made is unknown. We will see later if this could be a problem during the final assembly.

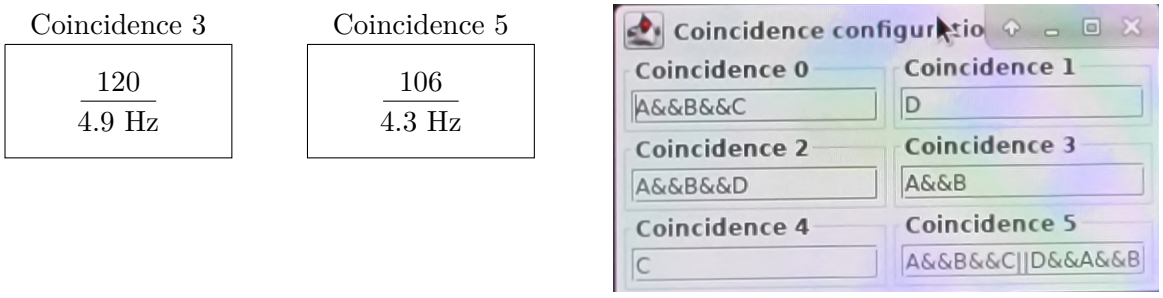

(a) (b)

Figure 25: (a) Coincidence counters, the values indicated are the number of detection and the frequency of detection. (b) Configuration of the coincidences, A and B correspond to the SiPMs on the tracking setup. C and D correspond to the two SiPMs placed on the scintillator whose efficienct is sought.

4 Measurements and simulations

4.1 Simulation of events

Before discussing the simulation used for this project, it should be noted that a simulation via Geant4 has been considered. **Geant4** (for **GE**ometry **AN**d **T**racking) is a software used mainly by CERN researchers , to simulate the interactions between particles and matter. However, given the complexity of the simulation, it was deemed unnecessary to use Geant4. Moreover, if we produced the simulation with Geant4, the simulation results come out (for ATLAS) as ROOT files, Root beeing a data analysis software also used by CERN. This made it even more difficult to use. The simulation was therefore carried out in C++ (and data analysis of results, in python), without using any particular libraries, except to generate random numbers. We used cstdlib, given the small number of numbers to generate, it was not necessary to use a more complex generator.

4.1.1 Simulation objectives

The main goal of our simulation was to reproduce the behavior of the scintillator (as well as the wrap it was in, which allowed the light to be confined), as well as the SiPM. To do this, we used available data concerning the materials, as well as the laws of physics we needed.

Physical model of the simulation

We used the laws of refraction of light, whose formula simply, for reflection (θ_i the angle of incidence, and θ_r the refraction angle):

$$\theta_i = \theta_r \tag{4}$$

This formula is valid up to a certain angle, called the **critical angle** below which all the light is reflected (with the refractive index of the medium n_1 for the material, and n_2 for the air) :

$$\sin(\theta_c) = \frac{n_2}{n_1} \tag{5}$$

As said before, the reflection does not only take place on the edges of the scintillator, but also on the wrapping. The light transmitted at the scintillator-air interface, then reflected at the level of the wrapping (Fig.26), and again transmitted at the air-scintillator interface also have an angle of reflection equal to that of incidence, the transmission having taken place one times in each direction.

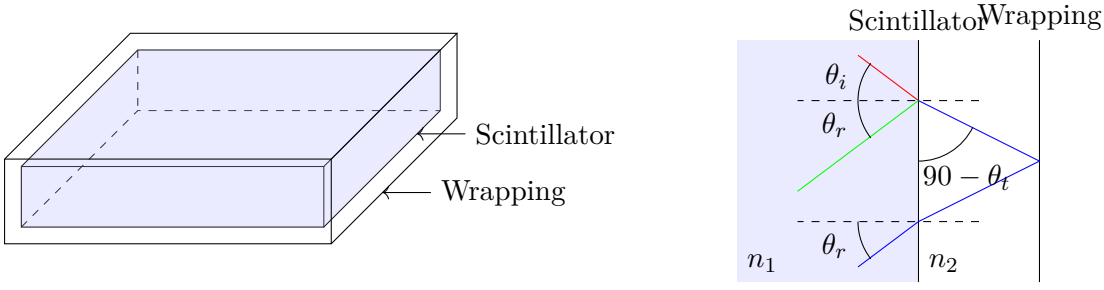

Figure 26: Diagram of the simulated environment. The incident beam is in red, the reflected one in green, and the transmitted one in blue. No light coming from outside is considered (the wrapping works like a mirror).

The code will not be presented directly here, but the principle of operation is shown in Fig.27.

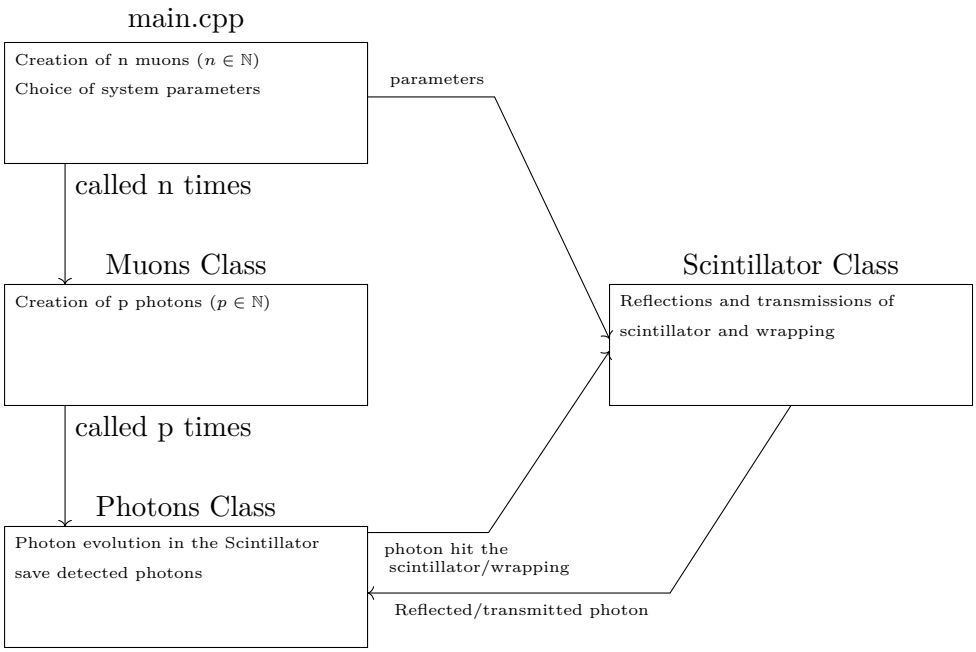

Figure 27: Diagram of the operation of the code allowing the simulation of muons/photons within the scintillator.

4.1.2 Results

Before discussing the plots used quantitatively, it is interesting to look for a moment at the "graphical" results of this simulation (Fig.28), which shows us how the photons behave within the scintillator. Only muons in normal incidence are considered.

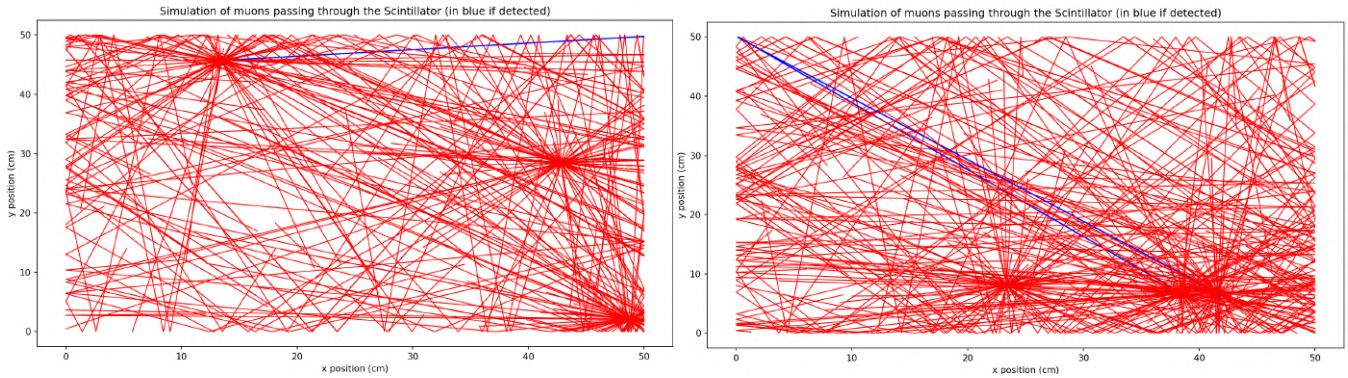

Figure 28: Projection on the x,y plane of the paths traveled by the photons within the scintillator. The photons appear in red, the muons (three for these examples) are discernible at the points of photon accumulations. If a photon is detected by one of the SiPMs (in the top-left and top-right corners) it appears in blue.

In Fig.28, we observe a variety of different paths of the photons, which does not seem, at first sight, to have a privileged direction. The z direction is not shown here because SiPMs can only be placed on the edges of the (x,y) plane. The photons that stop in the middle of the scintillator have either been absorbed by the top or the bottom of the scintillator, or by the material.

The first interesting qualitative result concerns the path length of the photons within the scintillator. If our simulation is consistent, we should obtain a exponential decreasing.

Indeed, we observe (Fig.29) an exponential behavior, which is consistent with the real behavior of photons within a material. One can see that a photon can travel up to 100 cm and more. Indeed, to achieve a coincidence, it is necessary to choose a time window during which two photons will be considered as coming from the same muon. However, if one of the photons travels 1 cm, and the other 100 cm, the time interval between the two can be greater than the time window. We will discuss the implications of this in more detail in the result section.

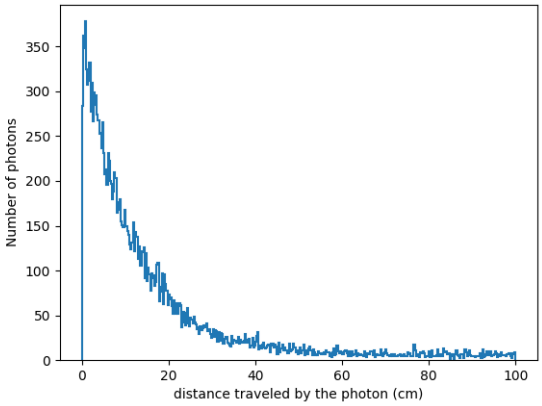

Figure 29: Distance traveled by a photon within the material in simulation. Histogram made with 500 muons.

We presented one of the results in Fig.15, however, in order to determine if the very high detection on the edge of the scintillator is indeed due to the increase in the solid angle of this position (and not to a simple discontinuity of the edges of the scintillator), it is useful to check (with the same data) the other side of the scintillator (Fig.30), which does not have the cuts on the angles.

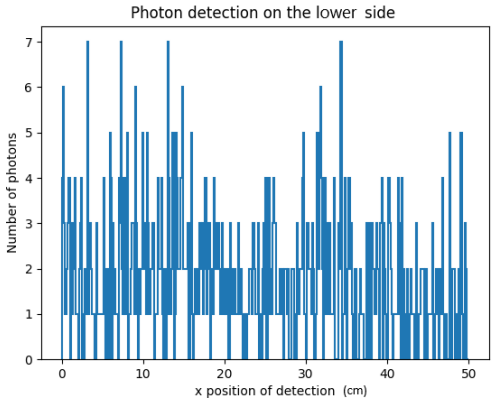

Figure 30: Simulated number of photons detected as a function of the position along the edge of the scintillator opposite to that studied in Fig.15.

We find (in Fig.30) the same values as in Fig.15 in the center, but without the very high values on the edges. This result confirms our hypothesis of the best position of the SiPMs.

The last use of this simulation comes from an idea that arose during a meeting. We now understand, from our results, that having cuts on the corners of the scintillators increases efficiency. However, it is not easy to place SiPMs on these corners. The idea therefore came to see if making larger corner, for example 1 cm, would have the same advantages, while making it easier to position the SiPMs.
We therefore launched the simulation, for 500 muons, in two different scintillators, one with 3mm corner (those of the real scintillators, Fig.31 on the left), and the other with 10mm corner (Fig.31 on the right).

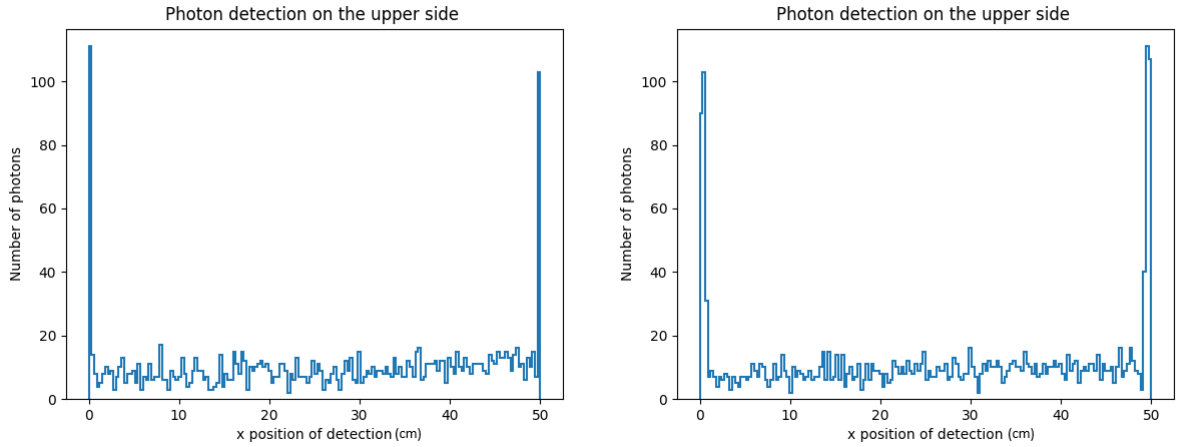

Figure 31: Comparison of photon detection with two scintillator, one with 3mm cuts on the corner, and the other with 10mm cuts on the corner. The simulation ran for 500 muons.

Fig.31 shows that the results look similar, but only in the center of the cuts, in the case of the 1 cm cuts. Positioning the SiPMs precisely would therefore also be more difficult than with the 3 mm cuts. That is why we didn't make the decision to enlarge the cuts.

4.2 Efficiency mesurement

4.2.1 Tracking setup

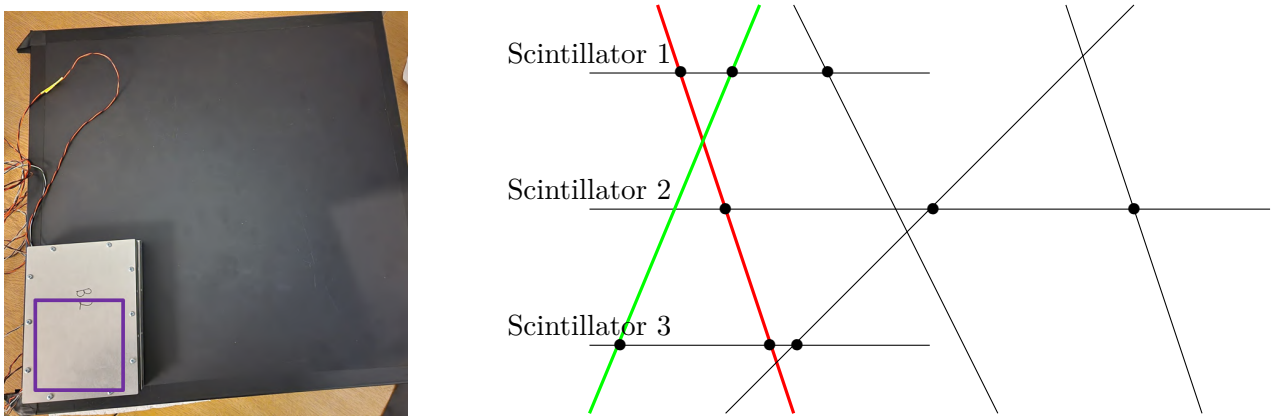

(a) (b)

Figure 32: (a) Picture of the device, the purple square represents the sensitive area, where the scintillators are (b) Operation of the tracking setup (with 10x10 cm^2 scintillators). The colors are taken from the coincidence in Fig.12.

The first experiment consists in measuring the efficiency of each scintillators, in order to verify the properties of the scintillators and the SiPMs (by placing a SiPM on each side of the scintillator, it is possible to verify that the results are indeed symmetrical).
In order to carry out the measurements, we used two other scintillators (already fully prepared with their SiPM, named Scintillator 1 and 3 on Fig.32) of 10×10 cm^2, which allowed me to make a kind of prototype of my final device (Shown in Fig.12), in order to measure the efficiency of the scintillators I use.

4.2.2 Results

After building and assembling all the SiPMs presented in section 3.1, we used the method presented previously to measure the efficiency of the scintillators. These results are measured with Ketek SiPMs. To start, we measured the efficiency of two scintillators (Fig.33), in order to check if the results are similar. Different results could come from a malfunction of certain SiPMs, or from a defect within a scintillator.

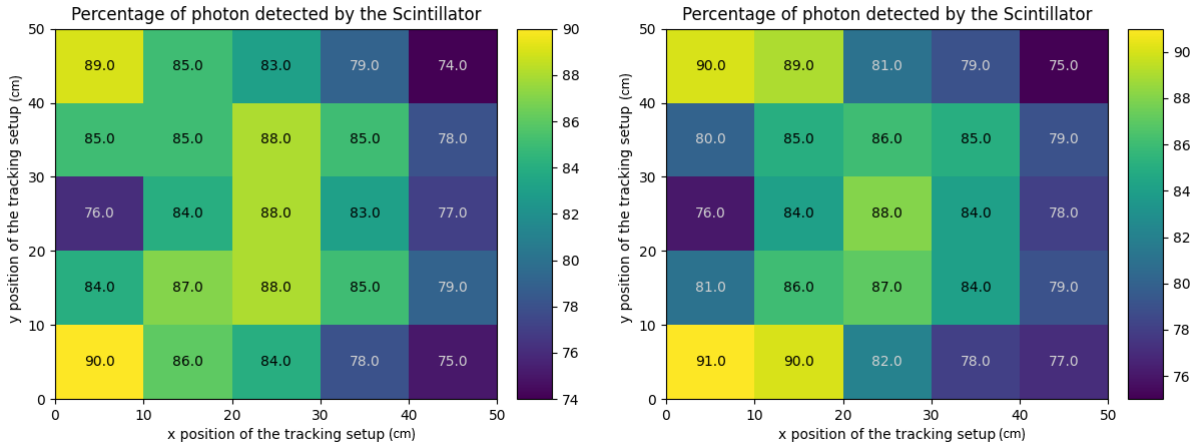

(Scintillator 2) (Scintillator 3)

Figure 33: Comparison of efficiency between two scintillators, 50×50 cm^2, number 2 and 3. The statistical uncertainty is 2%.

First, Fig.33 shows that the results are similar within the same Scintillator. Indeed, the SiPMs being placed at the top and at the bottom on the left, one observes a symmetry along the x axis. Then the results between the two scintillators are also symmetric. However, some values exceed the uncertainty (classical standard deviation calculated for 300 muons). These differences appear at places where the muons are less likely to be detected, because they are partly outside the detection cone of the SiPMs (the SiPMs will be more likely to detect what is in front of them).

The last scintillator, number 1, gives the same result. Here we will try to add optical grease between the SiPM and the scintillator, in order to check if better contact improves the efficiency of the system.
We observe in Fig.34 that the maximum efficiency (in the parts close to the SiPMs) does not change, however, the parts farther from the scintillator see their efficiency increased. It is understood that the photons arriving on the edge of the scintillator with a low angle will have a greater tendency to cross (and be detected) when optical grease is added.
In addition to all these efficiency measures, we also checked for any possible environmental impacts. That is to say the presence of external light, in different quantities, and the position of the electronics. We found no significant difference (exceeding the statistical uncertainty). This study guarantees us the efficient operation of the device.

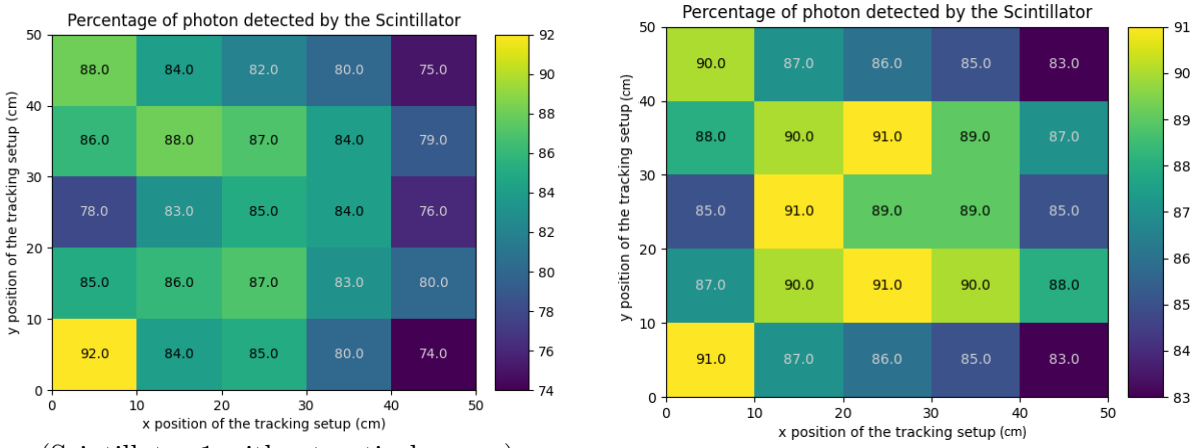

(Scintillator 1 without optical greese) (Scintillator 1 with optical greese)

Figure 34: Efficiency measurement after adding optical grease between the SiPM and the scintillator. The statistical uncertainty is 2%.

4.3 Final results

After all these measurements, the final device has been put in place, i.e. from now on, the tracking setup will no longer be done with the small scintillators, but with the large ones. The objective here is to measure the sensitivity over the whole scintillator, using two other scintillators to do the tracking setup. In order to adjust the threshold, it was decided for the threshold to put it as low as possible on the tracking setup around 700 mV (Fig.21), in such a way that we are certain to have only muons detected, and as little noise as possible. For the scintillator whose efficiency we want to know, it was decided to leave the threshold higher, so as not to lose certain muon signals in the middle of the noise.

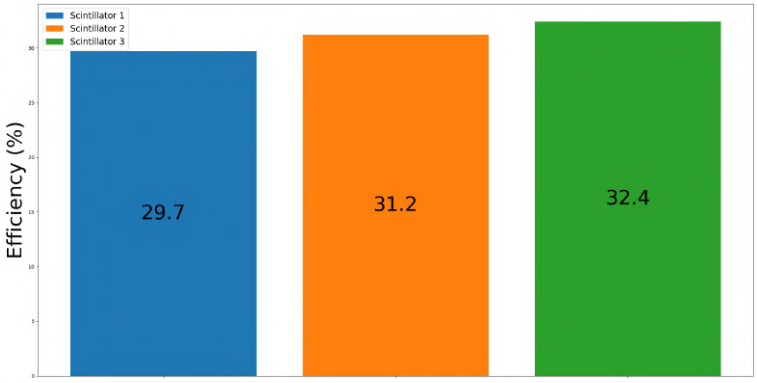

Figure 35: Measurement of the efficiency of the three scintillators (2% uncertainty).

How is it possible ? efficiency, compared to the last measurement, has dropped by 40% (Fig.35). Since this problem happened at the end of the internship, the question remained unanswered. However, we still had time to discuss possible explanations for this discrepancy between the measurements. First of all, we checked that the modifications made to the assembly did not affect the measurement, by resuming the old tracking setup, and checking that the efficiency had remained unchanged. Then, we checked the different boards, to verify that the tensions were consistent. After analyzing where the unexpected low results could come from, we noticed that the size of the scintillators could be the key to this problem.

Indeed, given the dimensions of a scintillator, the coincidence time window, which we briefly discussed during the presentation of the coincidence setup, might not be suitable. In a scintillator, a photon can go directly into the SiPM, or can perform several reflections before reaching it. The simulation tells us that a photon can easily travel 100 cm, which corresponds to 3 ns, at light speed. The attenuation length of the light being 380 cm (see Fig.22), one can reach 12.7 ns. If the coincidence time window is less than this value, many photons (and therefore muons) will not be considered coincidence, even though they are. The person knowing how to code the software not being there, we could not go further, also not having access to the code which could make it possible to modify this window of time of coincidence. Another solution would be a problem in coincidence logic, as we don't know the precedence rules of the AND and OR operators for the software.

5 Conclusion

Through this internship, using measurements and simulations, we were able to determine the best possible tracking setup, given the equipment we had, we thus chose the most efficient (and compatible) scintillators and SiPMs. We then found the best possible position for the SiPMs. Finally, we studied the coincidence setup, in order to optimize the device.
The final setup cannot be shown here as the mechanical part being not finished yet by the workshop. If our hypothesis for explaining the low efficiency of scintillators is true, it would suffices to increase the coincidence time window. The frequency of passage of the muons remains rather low and the noises also, that should not increase them significantly.
The simulation is not perfect, but very useful, because it allows us to answer many questions that we discussed during this internship. A possible improvement for this simulation would be to better reproduce the properties of the materials. The simulation considers an isotropic emission of the photons, but the direction of the muons can influence the emission of the photons (a cone formed in the direction of the propagation of the muons will be preferred).
From now on, the main challenges to solve are to regain the efficiency we had in Fig.33, as well as the installation of the elements on the mechanical part. This device will be used in the years to come, in order to measure the efficiency of the RPC detectors, which will soon arrive in the laboratory. We hope to be able to find efficient gases, with a low carbon footprint.
The prototype of ANUBIS will be ready within a few years, with the RPC detectors, and can (hopefully) be placed in PX14 (see Fig.1), and realise the first measurements. If everything works as expected, we can then build the actual detector, still using the device studied here, to measure the efficiency. Perhaps this is the beginning of the detection of new, long-lived particles that could validate or invalidate current theories, such as supersymmetry.

6 Appendix

6.1 Appendix A : LLP Models

In this section, we will attempt to develop supersymmetric motivations and theories involving long-lived particles. Of course, we will not go into all the technical details concerning supersymmetry, but we want to explain here why it is relevant to search for these particles, based on this theory.

As presented in the introduction, many problems reside within the standard model. We know that the Standard model is valid until a finite energy scale Λ. Take the Higgs potential (with $\mu, \lambda \in \mathbb{R}$) $V(H) = \mu^2 H^\dagger H + \lambda (H^\dagger H)^2$ we have, taking quantum fluctuation $\delta\mu^2 \sim \frac{\Lambda^2}{16\pi^2}$ (with Λ the cut-off parameter). We can also see the problem throught the top-quark loop contribution for the Higgs mass (using Feynman rules, with $c_t \in \mathbb{C}$, m_t the mass of the top quark and $\not{k} = \gamma^\mu k_\mu$, γ^μ being the Dirac matrices):

$$\delta m_\phi^2 = \frac{3i|c_t|^2}{2} \int \frac{\mathrm{Tr}((\not{p} + m_t)(\not{p} + m_t))}{(p^2 - m_t^2)^2} \frac{d^4p}{(2\pi)^4} = \frac{-3|c_t|^2}{2} \left(\Lambda^2 - 3m_t^2 \ln\left(\frac{\Lambda^2 + m_t^2}{m_t^2} \right) + \mathcal{O}(\Lambda^{-1}) \right)$$

Here Λ is used to regularise the integral, but its give us a corrected Higgs mass which is not of order 1.

One might see that this problem only affect scalar fields. Indeed, fermion and spin-1 fields have no hierarchy problem, since they break a symmetry.

Fermion spin-1 and scalar Lagrangian

The Lagrangien of these theories are (with m, λ, $\mu \in \mathbb{R}$ and $\not{\partial} = \gamma^\mu \partial_\mu$) :

$$\mathcal{L}_{\text{spin-1}} = -\frac{1}{4} F^{\mu\nu} F_{\mu\nu} + \frac{1}{2} m^2 A_\mu A^\mu \quad \text{and} \quad \mathcal{L}_{\text{fermion}} = i\overline{\psi}\not{\partial}\psi - m\overline{\psi}\psi$$

The scalar lagrangian is :

$$\mathcal{L}_{\text{scalar}} = \frac{1}{2}(\partial_\mu \phi)(\partial^\mu \phi) - \frac{1}{2} m^2 \phi^2 - \frac{1}{6}\mu\phi^3 - \frac{1}{24}\lambda\phi^4$$

It is easy to see that the two first Lagrangians obtain a symmetry when taking the massless case (gauge transformation $A_\mu \to A_\mu + i\partial_\mu \Lambda$, $\partial^\mu \partial_\mu \Lambda = 0$ for the first, and chiral transformation $\psi \to e^{ig\gamma_5}$, $g \in \mathbb{R}$ for the second). With the exception of the Nambu-Goldstone bosons, the scalars have no additional symmetry when taking the massless limit. The idea to solve this problem would be to consider a new field, interacting with the Higgs and making it possible to compensate for the divergences of the standard model.

Therefore, we also need a new symmetry that we will break later. Starting from the Poincaré group, the only way to find new symmetry is dictated by the Coleman-Mandula theorem.

Coleman-Mandula theorem

Theorem : There is no interacting quantum field theory with a mass gap where spacetime and internal symmetries are combined in a nontrivial way.

Therefore, except the generators of the Poincaré groups, the other conserved quantities must be Lorentz scalar. If we want to add a new generator G^a we must have (P_μ and $J_{\mu\nu}$ the generators of the Poincaré algebra) :

$$[P_\mu, G^a] = [J_{\mu\nu}, G^a] = 0$$

The theorem can also be expressed in a different, more general matter, which tells us that for our theory, any generalization of the Poincaré group will be a direct product between the Poincaré group and another group. The Lie algebra will be a direct sum between the Poincaré algebra and that of the other group.

Supersymmetry uses the only possible loophole, using fermionic generators, and constructing the Super-Poincaré algebra. We will not study these supersymmetric theories in more detail. We will now look for the different ways to break this symmetry.
The easiest way to break symmetry, which does not involve gravity, is gauge-mediated supersymmetry breaking.
The theory is broken throught the superpotential ($\lambda_{ij} \in \mathbb{R}$) :

$$W = \lambda_{ij}\bar{\phi}_i X \phi_j$$

Equation from Ref.[11]. This superpotential interaction between the chiral messenger superfield (ϕ) and the goldstino superfield X.
The goldstino superfield X acquires a vacuum expectation value (along the scalar and auxilary components) when SUSY is broken :

$$\langle X \rangle = M + \theta^2 F$$

Equation from Ref.[11]. Here, M is the messenger mass scale, and F is proportional to the mass-squared splitting inside the supermultiplet. $\sqrt{F}$ represent the measure of the supersymetry breaking in the messenger sector. In this theory, the mass of the new particles, and therefore their lifetime will depend on F. There can therefore be particles with a long lifetime, this is the case for example of neutralinos, presented in Fig.6.
We won't present all the other models, but another interesting one is split-SUSY. In this theory, all scalar particles are very heavy, and SUSY breaking happens at very high energy, except for a single particle (gluino). It is easy to see that this explanation lies in the absence of observation of supersymmetric particles, which makes us think that they are (if they exist) at very high mass scales. This model solves some problems, and creates a long-lived particle (the gluino), but it does not solve the mass hierarchy problem.

6.2 Appendix B : Critical angle

We will develop here a demonstration of the formula for the critical angle, used for our simulation.

Considering two dielectric material (with different refractive indice).

Planes waves

We consider plane waves for the incident (i), reflected (r) and transmitted (t) beam:

$$\vec{E}_i = \vec{E}_{i0} e^{i(\vec{k}_i.\vec{r}-\omega_i t)}$$
$$\vec{E}_t = \vec{E}_{t0} e^{i(\vec{k}_t.\vec{r}-\omega_t t)}$$
$$\vec{E}_r = \vec{E}_{r0} e^{i(\vec{k}_r.\vec{r}-\omega_r t)}$$

In our calculation, $(\vec{e}_x, \vec{e}_y)$ will be the **incident plane**, with $\vec{e}_x$ parralel to the interface, and $\vec{e}_y$ perpendicular to it.

We will use here the relations at the interfaces for the dielectrics for the E and B fields.

Recall: General interface conditions

In general, we have, for the Electric field strength E, Electric displacement field D, magnetic flux density and magnetic field strength :

$$\vec{n}_{12} \wedge (\vec{E}_1 - \vec{E}_2) = \vec{0} \qquad \vec{n}_{12}.(\vec{D}_1 - \vec{D}_2) = \sigma$$
$$\vec{n}_{12}.(\vec{B}_1 - \vec{B}_2) = 0 \qquad \vec{n}_{12} \wedge (\vec{H}_1 - \vec{H}_2) = \vec{j}$$

With $\vec{j}$ the surface current density, σ the charge surface density. $\vec{n}_{12}$ correspond to the normal vector of the interface plane (between two medium with a refractive index n_1 and n_2).

We use here the continuity of the electric field:

$$E_{ix}+E_{rx} = E_{tx} \Longrightarrow E_{i0}\cos(\theta_i)e^{i(k_i x \sin(\theta_i)-\omega_i t)} - E_{i0}\cos(\theta_r)e^{i(k_r x \sin(\theta_r)-\omega_r t)} = E_{i0}\cos(\theta_t)e^{i(k_t x \sin(\theta_t)-\omega_t t)}$$

We consider now $\omega_i = \omega_r = \omega_t$ (as the relation above is true for all t), and $k_i x \sin(\theta_i) = k_r x \sin(\theta_r) = k_t x \sin(\theta_t)$ (same argument but with x).
Using $k = \frac{n\omega}{c}$, and the previous relation, we found:

$$\theta_i = \theta_r \quad \text{and} \quad n_1 \sin(\theta_i) = n_2 \sin(\theta_t)$$

Note that we have also just demonstrated (first equation) the equality between the angle of incidence and reflection, which we use in our simulation. The second equation tells us that it is not possible to exceed a certain angle, when $n_1 > n_2$ (because $\sin(\theta_t)$ cannot exceed 1 when $\theta_t \in \mathbb{R}$). We will call this limiting angle the **critical angle**:

$$\sin(\theta_c) = \frac{n_2}{n_1}$$

6.3 Appendix C : Wrapping

For the materials to be used, we chose aluminum foil, which seemed to have the best price-quality ratio (Fig.36). The surface (scintillator side) is polished, hence the use of the formula : $\theta_i = \theta_r$.
Another possible choice would have been to tarnish the surface, which would have given a random reflection angle in the simulation, but that didn't seem to be the best solution, so we choose to stay with the basic, polished wrap.

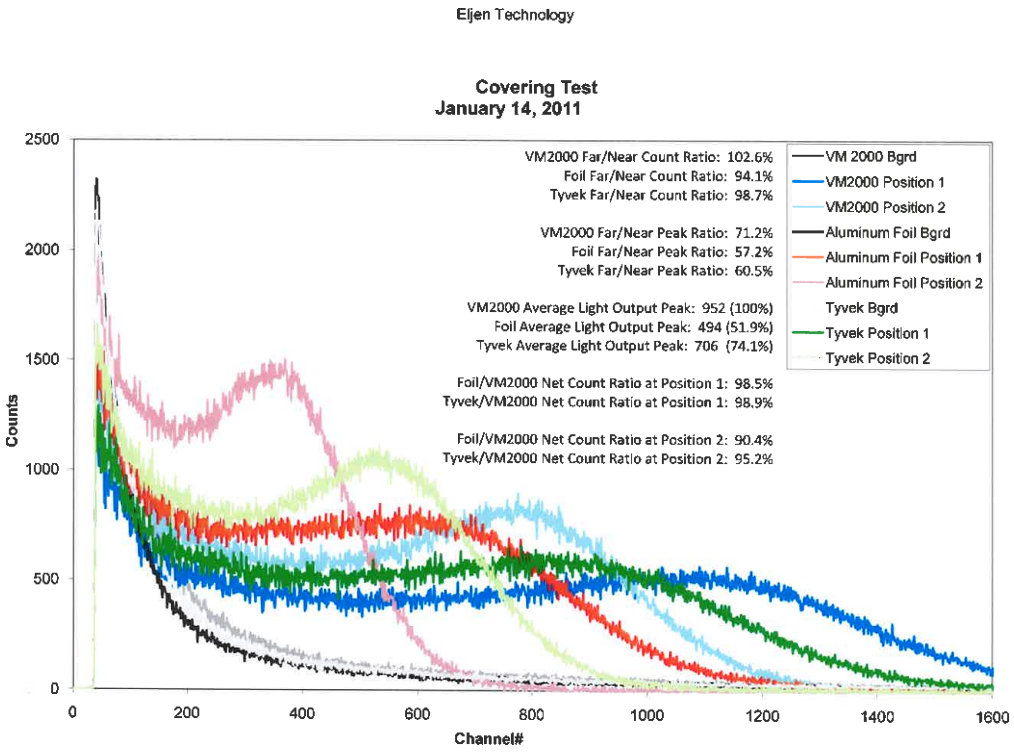

Figure 36: Test of different materials for wrapping around the scintillator.

6.4 Appendix D : Cosmic muons

Permanently, the air on Earth is traversed by a flow of particles, coming from space (stars, black holes, etc.). This flow of particules is called cosmic radiation, and was found by Victor Hess (Nobel Prize, 1936).

In addition to the photons that come to us from space (and allow us to observe the stars), other particles, such as pions, muons, and proton pass through the atmosphere. Protons are the majority in cosmic rays, in the part called Primary Cosmic Rays. They then interact with the atmosphere, mainly to form pions (as well as other less probable reactions), these pions will then, if their energy allows them, disintegrate into muons and muonic neutrinos. Height scales are given in Fig.37 in order to know where his interactions take place, on average.

Fig.36 shows that the main particles managing to reach the ground are neutrinos and muons (ν_μ and μ^-). As scintillators are sensitive to charged particles, we are more interested in muons here. Muons have a very short lifetime of $2.2\,\mu s$ (value taken from ref.[12], chapter 4). However, this time is sufficient to reach the ground, even at sea level.

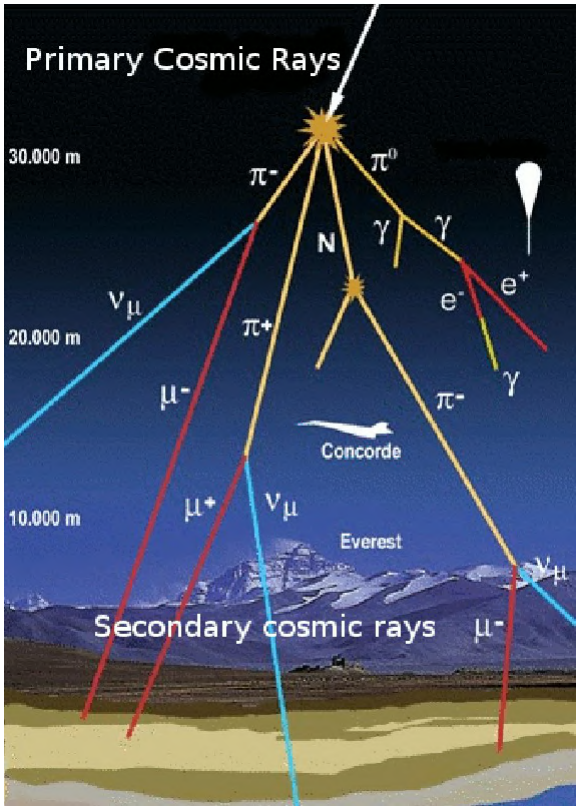

Figure 37: Feynman diagram of the production (after interaction with the atmosphere) of secondary Rays. Figure from Ref.[13]

Muons arrive on earth at different angles from the zenith (Fig.38), which changes their average momentum. This is because pions with high momentum are more likely to decay into muons before interacting with the atmosphere (which does not filter in the same way at each location), giving rise to muons also at high momentum.

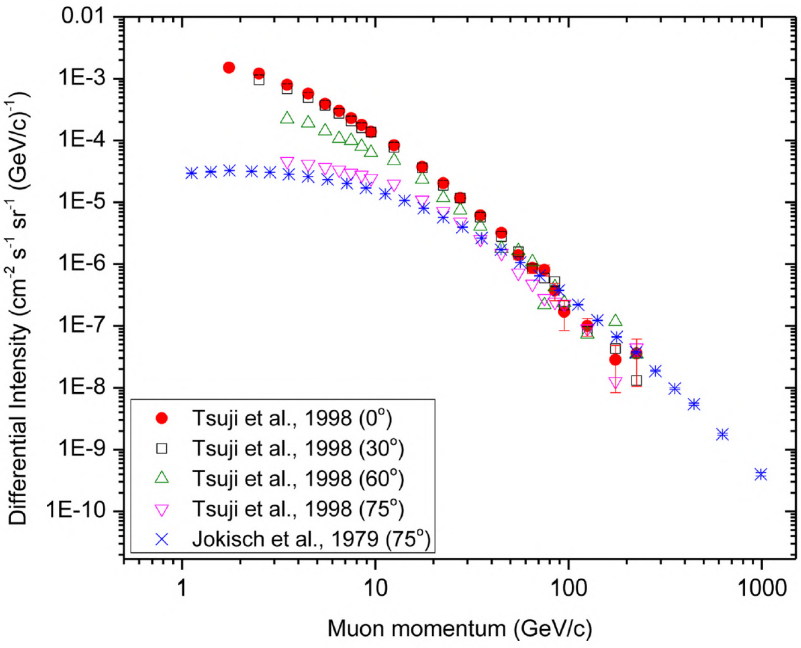

Figure 38: Measured muon momentum spectrum at sea level, for different angles from the zenith. Figure from Ref.[12]

Muons therefore seem to be the best particles to use in our study, given their abundance as well as their charge, which allows them to be easily detected, using scintillators, or RPCs. We have not discussed here of the frequency of muons reaching sea level. Our experiments shows that every second, dozens of muons are passing through our scintillators, which allows us, among other things, to greatly reduce the uncertainty in our measurements.

Glossary

ANUBIS : An Underground Belayed In-Shaft search experiment

ATLAS : A Toroidal LHC ApparatuS

BSM : Beyond the Standard Model

CERN : Conseil Européen pour la Recherche Nucléaire

DCR : Dark Count Rate

Geant4 : GEometry ANd Tracking 4

HEP : High Energy Physics

LHC : Large Hadron Collider

LLP : Long-Lived Particles

PDE : Photon Detection Efficiency

RPC : Resistive Plate Chambers

SiPM : Silicon Photomultiplier

SM : Standard Model

SUSY : Supersymmetry

Bibliography

[1] Martin Bauer, Oleg Brandt, Lawrence Lee, and Christian Ohm. Anubis: Proposal to search for long-lived neutral particles in cern service shafts, 2019. https://arxiv.org/abs/1909.13022.

[2] Vladimir V. Gligorov, Simon Knapen, Michele Papucci, and Dean J. Robinson. Searching for long-lived particles: A compact detector for exotics at LHCb. *Physical Review D*, 97(1), jan 2018. https://arxiv.org/abs/1708.09395.

[3] John Paul Chou, David Curtin, and H.J. Lubatti. New detectors to explore the lifetime frontier. *Physics Letters B*, 767:29–36, apr 2017. https://doi.org/10.1016%2Fj.physletb.2017.01.043.

[4] Lawrence Lee, Christian Ohm, Abner Soffer, and Tien-Tien Yu. Collider searches for long-lived particles beyond the standard model. *Progress in Particle and Nuclear Physics*, 106:210–255, may 2019. https://arxiv.org/abs/1810.12602.

[5] M. Aaboud and al. Search for long-lived particles produced in pp collisions at $\sqrt{s} = 13$ TeV that decay into displaced hadronic jets in the ATLAS muon spectrometer. *Physical Review D*, 99(5), March 2019. https://arxiv.org/abs/1811.07370.

[6] Vincent Français. *Description and simulation of the physics of Resistive Plate Chambers*. PhD thesis, July 2017. https://www.researchgate.net/publication/323687584_Description_and_simulation_of_the_physics_of_Resistive_Plate_Chambers.

[7] ELJEN TECHNOLOGY. *General Purpose Plastic Scintillator EJ-200, EJ-204, EJ-208, EJ-212*, July 2021. https://eljentechnology.com/products/plastic-scintillators/ej-200-ej-204-ej-208-ej-212.

[8] sensL. *An Introduction to the Silicon Photomultiplier, technical note*, February 2017. https://cernbox.cern.ch/index.php/s/1NSCluoAatGCMZu.

[9] Ketek. *Product Data Sheet SiPM Silicon Photomultiplier PM3315-WB-B0*, Rev. 12/2018. https://www.ketek.net/wp-content/uploads/2018/12/KETEK-PM3315-WB-B0-Datasheet.pdf.

[10] Broadcomő. *AFBR-S4N33C013 NUV-HD Single Silicon Photo Multiplier*, January 4, 2022. https://docs.broadcom.com/doc/AFBR-S4N33C013-DS.

[11] G.F. Giudice and R. Rattazzi. Theories with gauge-mediated supersymmetry breaking. *Physics Reports*, 322(6):419–499, dec 1999. https://arxiv.org/pdf/hep-ph/9801271.pdf.

[12] Floris Keizer. *Sub-nanosecond Cherenkov photon detection for LHCb particle identification in high-occupancy conditions and semiconductor tracking for muon scattering tomography*. PhD thesis, Churchill College, University of Cambridge, June 2019. https://www.repository.cam.ac.uk/handle/1810/298766?show=full.

[13] Francisco Barradas-Solas. Giving new life to old equipment. *Physics Education*, 42(1):9–11, January 2007. https://www.researchgate.net/publication/243676392_PARTICLE_PHYSICS_Giving_new_life_to_old_equipment.